Single-particle motion in three-dimensional vibrofluidized granular beds

R. D. Wildman,[1] J. M. Huntley,[1] J.-P. Hansen,[2] D. J. Parker,[3] and D. A. Allen[3]
[1]*Department of Mechanical Engineering, Loughborough University, Loughborough, Leicestershire LE11 3TU, United Kingdom*
[2]*Department of Chemistry, University of Cambridge, Lensfield Road, Cambridge CB2 1EW, United Kingdom*
[3]*School of Physics and Astronomy, University of Birmingham, Edgbaston, Birmingham B15 2TT, United Kingdom*
(Received 30 March 2000)

A technique to probe the interior of three-dimensional dynamic granular systems is presented. Positron emission particle tracking (PEPT) allows a single tracer particle to be followed around a three dimensional vibrofluidized granular bed for periods up to six hours. At present the technique is able to resolve the position of the grains to ± 4 mm, with an average temporal resolution of about 7 ms. Packing fraction profiles are calculated by making use of the ergodicity of the system, and granular temperature profiles are obtained, in the dilute case, from the short time behavior of the mean squared displacement. At longer times, the mean squared displacement shows a range of behavior which can be explained by the presence of strong gradients in the packing fraction. Convection currents were observed, but were sufficiently small in magnitude to be ignored during the analysis of grain motion. The system was modeled using the Smoluchowski equation, which was solved numerically, and the results compared with the experimentally determined displacement probability density functions. Good agreement between experiment and numerical results was achieved using Brownian motion relationships modified to accommodate differences between granular systems and thermal systems.

PACS number(s): 45.70.Mg, 51.10.+y, 05.40.−a, 05.60.−k

I. INTRODUCTION

Granular materials have been studied closely by scientists and engineers for over a hundred years. The ubiquity of such materials in both nature and industry has precipitated many studies with the aim of improving transportation and storage methods. Recently, the complexity and richness of the behavior of dissipative and nonequilibrium systems has led to renewed interest in granular flows at the microscopic or single-particle level. On the whole, the investigations have centered on theoretical and numerical analysis of the problem. For example, Savage and Jenkins pioneered the use of kinetic theory methods to model microscopic motion in granular flow [1], and McNamara and Luding have studied dissipative systems using molecular dynamics (MD) and event driven simulations [2]. The need for experimental validation of these approaches was emphasised by Campbell in his review paper [3]. In response to this, a number of phenomena have been systematically investigated, including convection [4], gravity driven flows [5] and wave propagation [6]. Generally, experimental investigation of granular systems has concentrated on two-dimensional systems (see, e.g., Ref. [7]), but recently a range of techniques has been used to observe motion in three dimensions, including magnetic resonance imaging [8], diffusive wave spectroscopy [9], and positron emission particle tracking [10].

Theoretical descriptions of granular flows have generally used kinetic theory methods analogous to the Chapman-Enskog approach to atomic gases. Jenkins and Richman analyzed the case of nearly elastic, hard disk gases [11], and a similar analysis was undertaken by Kumaran to describe vibrofluidized granular beds [12]. Essentially, this method relies on expanding the velocity distribution into its moments, with the Maxwell-Boltzmann distribution forming the leading term in the approximation. Comparison with numerical studies has indicated good agreement, but experimental validation has yet to be performed for three-dimensional systems. Kinetic theories have also been used to produce sets of hydrodynamic equations appropriate to granular flows [13].

Model two-dimensional vibrofluidized granular beds of steel spheres (restitution coefficient, $\varepsilon = 0.92$) were used in Ref. [7] to investigate the steady state behavior of a ''granular gas.'' High speed digital photography, together with image analysis and particle tracking software, was used to determine large numbers of particle trajectories and hence obtain velocity distributions. These authors showed that the velocity probability density function of such grains in a two-dimensional vibrofluidized granular gas closely corresponds to a Maxwell-Boltzmann distribution, and developed a method of extracting the granular temperature based on the fitting of the theoretical form of the velocity probability density to the experimentally acquired data [14]. By this method, granular temperature profiles in vibrofluidized beds were determined for the first time. Further, it was shown that apart from the accentuated influence of gravity, a highly fluidized granular system can behave in a fundamentally similar manner to a thermal fluid [15]. This method for determining granular temperature is appropriate at low or intermediate packing fractions, but at high densities ($\eta > 0.5$) the collision rate of the grains is of the order of the framing rate of most high speed video cameras (1000 frames per second for the study described above). To avoid this problem, a new method was suggested that relied on the analysis of the short time behavior of the mean squared displacement [16]. This method allowed measurement of granular temperature up to packing fractions approaching 0.8. Subsequently, the measurement of the granular temperature, combined with the determination of the self-diffusion coefficient from the same data, indicated that the Chapman-Enskog predictions used to relate the granular temperature to self-diffusion in granular gases were accurate to within 10–20 % for packing fractions up to about 0.6 [17]. This validation of the Chapman-Enskog

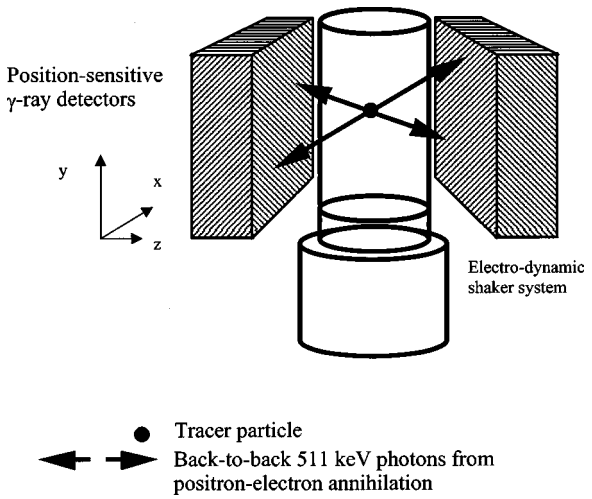

FIG. 1. Schematic of the PEPT facility.

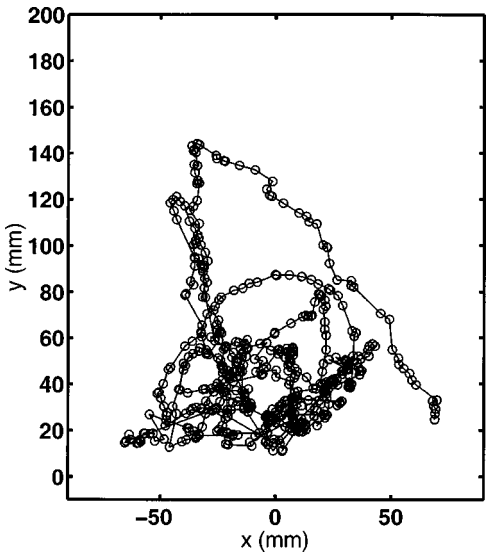

FIG. 2. First 500 location events for $N=700$. The positions are projected onto the x-y plane.

results up to $\eta \sim 0.6$ showed that measurement of self-diffusion coefficients could be used as an indirect way of measuring granular temperature [17].

The purpose of this paper is to present results from experiments on three-dimensional vibrofluidized beds performed using the positron emission particle tracking (PEPT) facility at the University of Birmingham, U.K. The PEPT experimental facility is introduced in Sec. II. Section III describes the measurement of packing fraction, displacement probability density functions, and mean squared displacement. Finally in Sec. IV, displacement probability density functions are compared with numerical solutions of the Smoluchowski equation.

II. EXPERIMENTAL PROCEDURE

Whole field methods of analyzing three-dimensional granular beds are not generally available, primarily because techniques such as high speed photography are unable to probe beyond the surface of the bed. Although PEPT tracks only a single radioactively labeled tracer particle, the automated facility allows experimental data to be logged for a considerable length of time (up to 6 h), allowing pseudo-whole-field data to be accumulated. The technique has recently been used to investigate a number of experimental situations, e.g., rotating beds [10] and paste flow [18], and it is clear that such a system has good potential for observation of grain motion in a three-dimensional vibrofluidized granular bed.

The tracer particle is prepared such that it contains a radionuclide that decays through positron emission. Annihilation of a positron upon encountering an electron produces a pair of back-to-back γ rays. These high energy photons are very penetrating, and an accurate location can be determined from detection of a small number of back-to-back pairs (see Fig. 1). From a series of such measurements the tracer location can be determined by triangulation, but it is necessary to collect enough data so that the background (due to, for example, scattered γ rays) can be distinguished. An iterative algorithm [19] is used to eliminate this background. This method typically requires 100 coincidence pairs for each location, which limits the timing resolution of the present system to about 4 ms. The detectors consist of a pair of multiwire proportional chambers each with an active area of $600 \times 300\,\mathrm{mm}^2$ [20]. In this study ballotini radiotracers were produced through their irradiation by ^{3}He nuclei; these were physically indistinguishable from the remaining beads within the experimental cell.

A three-dimensional granular gas was generated using a Ling Dynamic Systems (LDS) vibration system. A sinusoidal signal was fed through a field power supply (LDS FPS 1) and power amplifier (LDS PA 1000) into a wide frequency band electrodynamic transducer (LDS V651). This system has a frequency range of 5–5000 Hz, a maximum acceleration of 100 g and maximum amplitude of 12.5 mm. A cell of dimensions 140-mm diameter and 300-mm height was placed on the upper surface of the vibrating piston, itself placed between the photon detectors (Fig. 1). The cell was constructed of polymethyl methacrylayte to limit the attenuation of the γ rays as they travelled through the experimental apparatus. Glass ballotini balls of diameter 5.0 ± 0.2 mm (with a restitution coefficient ε, measured using high speed photography, of 0.91) were used as the granular medium.

At grain speeds of $\overline{c} = 1\,\mathrm{m\,s^{-1}}$, the PEPT camera has an accuracy of about ± 4 mm. The accuracy in the z direction is substantially worse (by a factor of about 3) as the grain needs to be located in a direction normal to the faces of the detectors. As the experimental arrangement was symmetrical about the cylinder axis, the form of the behavior in the z direction was assumed to be the same, on average, as that in the x direction, thereby eliminating a large source of error. The motion of a grain was followed for about 1 h, resulting in up to 3 000 000 location events. The number of grains, N, placed within the cell (including the tracer particle) was varied over the following set of values: 300, 700, 1150, 1400, 1750, 2100, 2450, 2800, 3500, and 4200, corresponding to a total number of grain layers varying from 0.5 to 6. For the experiments containing $N = 700$–4200 grains, the cell was vibrated at a frequency of 50 Hz and an amplitude of 1.91 mm; for $N = 300$, the same frequency and an amplitude of 2.10 mm were used. Figure 2 shows, as an example, the first 500 location events for the case $N = 700$ grains.

III. DATA ANALYSIS

A. Packing fraction

The constraints acting on the PEPT facility mean that only a single particle can be tracked at a time. Consequently, packing fraction cannot be calculated directly. However, if the system is ergodic then a time average is equivalent to an ensemble average, enabling the packing fraction to be measured indirectly through measurement of the residence time fraction (a proof of which, valid for an equilibrium system, is outlined in the Appendix). We have proceeded on the assumption that, as previous experiments have shown a close analogy between vibrofluidized granular beds and thermal fluids, that this will also be valid for nonequilibrium steady states.

Prior to determining the packing fraction, the experimental cell region was split into volume elements. These volume elements consisted of horizontal slices through the experimental cell at 5-mm intervals. The distribution function describing the probability of a grain being located in each slice was then determined. The reliability of a location event is dependent on the speed of the grain and the density of material at that location: the number of coincidence events, and thus the interlocation time interval, therefore varies. A more accurate representation of the packing fraction profile is to weight the location probability density by the *time* spent in each slice. The fractional residence time is calculated by recording the time between successive location events, apportioning the appropriate fraction of time to each slice if the grain has moved beyond its initial slice, summing the total time in each segment and normalizing to a total of one. The number density $n(y)$ can be approximated by

$$n(y)=\frac{NF(y)}{V_s}, \tag{1}$$

where N is the total number of grains, $F(y)$ is the residence time fraction of a grain in a segment, and V_s is the volume of a segment. The packing fraction $\eta(y)$ is given by

$$\eta(y)=n(y)\frac{\pi d^3}{6}, \tag{2}$$

where d is the grain diameter and the segment volume is given by

$$V_s=\Delta y\frac{\pi d_c^2}{4}, \tag{3}$$

where Δy is the segment thickness and d_c is the experimental cell diameter.

Combining Eqs. (1), (2), and (3) leads to the expression

$$\eta(y)=\frac{2}{3}\frac{NF(y)d^3}{\Delta y d_c^2}, \tag{4}$$

where y is the height above the base of the cell. The discrepancies between using the location probability density, and weighting by the time interval between locations, are however, relatively minor, corresponding to peak differences of around 1% in the packing fraction at $y\sim 20$ mm. In this paper, the residence time fraction is used due to the more accurate representation of the packing fraction profiles, but weighting could be omitted if rapid estimation of the packing fraction was required.

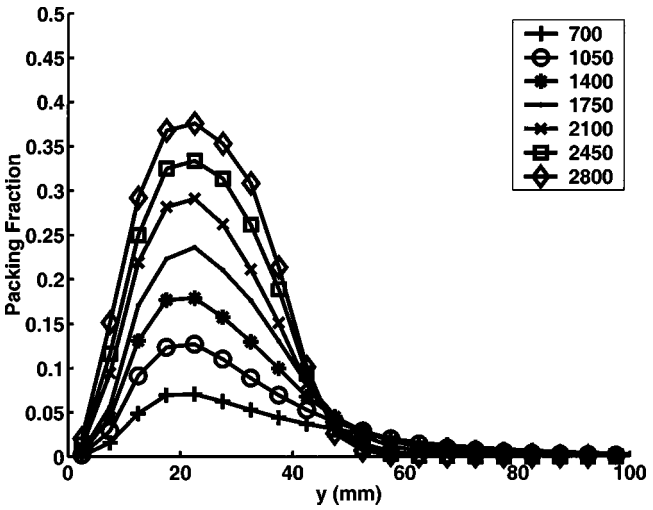

FIG. 3. Packing fraction profiles for $N=700-2800$.

Figure 3 shows packing fraction profiles from $N=700$ to 2800. These curves clearly differ from the exponentially decaying packing fraction profile, characteristic of an elastic gas in thermal equilibrium at low packing fractions. Rather, a ''humped'' profile is observed, aspects of which resemble packing fraction profiles measured using two dimensional granular gases [14]. MD simulations on hard inelastic discs show that the effect of large numbers of grains is to cause saturation of the packing fraction profile near the base [21]. The downturn in $\eta(y)$ below $y=10$ mm therefore seems likely not to be caused by the high excluded volume, but by the dissipation and energy flow from the base. The same data plotted on semilog axes (Fig. 4) demonstrate that at large values of y ($y>50$ mm) the packing fraction decays approximately exponentially, reflecting the reduced influence of the base on the motion of the grains at high altitudes. The asymptotic gradient, and hence granular temperature, is seen to decrease systematically with increasing values of N.

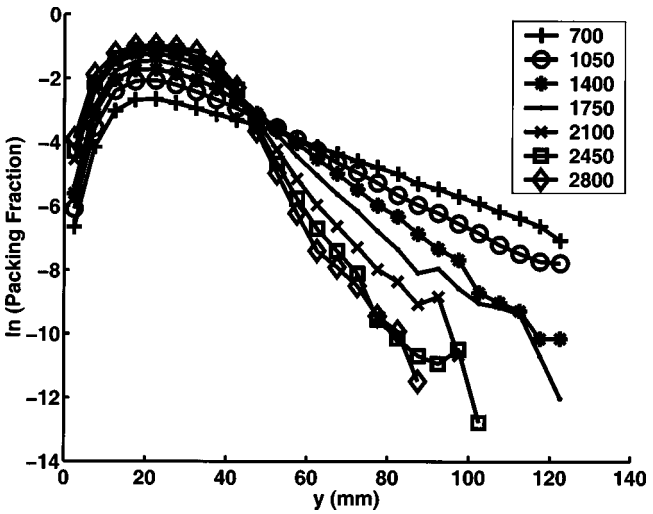

FIG. 4. Packing fraction profiles for $N=700-2800$, on semilog axes.

TABLE I. Standard deviation of the packing fraction σ_η, measured in 3×3 subregions within a 5-mm slice centered at a height $y=30$ mm above the base, for a range of grain numbers, N.

N	700	1150	1400	1750	2100	2450	2800	3500	4200
σ_η/η (%)	2.65	2.05	2.89	3.27	3.41	5.35	5.60	8.41	10.22

The ergodicity of the system was tested by splitting each slice into a 3×3 matrix of nine further segments, allowing the standard deviation in packing fraction across a plane to be determined. This analysis showed that when the system is dilute the variation is $<5\%$ and the full volume of the system is in effect explored by each grain over the time scale of each individual experiment (about 1 h). At very high packing fractions, e.g., when $N=4200$, the packing fraction is more variable, suggesting that the tracer requires significantly longer times than at low densities to explore the full volume of the system. Table I illustrates the variability (standard deviation) in the packing fraction at $y=30$ mm for each experiment. It was found that the variation was within 10% up to about $N=3500$, suggesting that the assumption of ergodicity is reasonable for $N\leqslant3500$.

A simple way of accounting for the excluded volume effects associated with the closely packed grains is to incorporate the radial distribution function at contact, $g_o(d)$, into calculations of the mean free path [22]. This has the consequence of modifying the mean free time between collisions, τ_E, such that

$$\tau_E=\frac{2}{nd^2\overline{c}g_o(d)}. \tag{5}$$

The radial distribution at contact is approximated in the manner suggested by Carnahan and Starling [23]:

$$g_o(d)=\frac{(2-\eta)}{2(1-\eta)^3}. \tag{6}$$

B. Displacement probability density

In an unbounded isotropic system no particular direction of movement is favored above any other. In such systems, in three dimensions, the probability of finding a grain in a volume element $d\mathbf{r}$ around the point $\mathbf{r}$ at time t, assuming the grain was at the origin at time zero, is governed by the diffusion equation

$$\frac{\partial u}{\partial t}=D\frac{\partial^2 u}{\partial \mathbf{r}^2}, \tag{7}$$

the solution of which is

$$u(r,t)=\frac{1}{(4\pi Dt)^{3/2}}\exp\left(-\frac{r^2}{4Dt}\right), \tag{8}$$

where u is the displacement probability density, D is the self-diffusion coefficient, and $r=|\mathbf{r}|$. The mean squared displacement can be calculated from Eq. (8) using the equation

$$\langle|\mathbf{r}(t)-\mathbf{r}(0)|^2\rangle=\int r^2u(r,t)d\mathbf{r}, \tag{9}$$

which leads to Einstein's relation

$$\lim_{t\to\infty}\frac{1}{6t}\langle|\mathbf{r}(t)-\mathbf{r}(0)|^2\rangle=D. \tag{10}$$

In a vibrofluidized bed a stochastic description of the motion is complicated by the fact that each grain is accelerated by gravity between collisions, and that D varies with position and (in two and three dimensions) depends on direction. The more complex partial differential equation (PDE) describing this situation, and its solution, is described in more detail in Sec. IV.

The experimental displacement probability density function is measured by calculating the distance moved by a grain following each location event. To attain good spatial resolution the experimental cell volume is split into slices, following the procedure established during the measurement of the packing fraction: the system is first analyzed by running through the location data in each run, assigning a number to each location event, and determining which slice the location event was found in. To reduce the effect of grain collisions with the side walls, only grain points located within a disc of diameter (d_c-15) mm are tracked. Each slice is then considered in turn, with every location event assigned to a slice considered as a starting location. For the location events succeeding each starting location, the displacement vector relative to the starting location is calculated. Thus, for each slice, a large number of individual displacements are determined for known times. These data are binned into both discrete times and displacements to create displacement probability densities within known time intervals. Figures 5(a) and 5(b) show typical probability densities for measurements made in the x and y directions. The approximately Gaussian form of the function in the x direction indicates that neither boundaries nor gravitational effects play a significant role in the behavior of the grains, over the time scale of the experiments shown in Fig. 5(a). However, in the y direction, the probability density is not in general Gaussian, nor does it tend to be symmetrical after short times. An explanation for this ''anomalous'' behavior is discussed in Sec. IV.

C. Mean squared displacement

The mean squared displacement can be calculated from the displacement probability density (Sec. III B) or directly from the experimental position data. In studies of two-dimensional vibrofluidized granular beds, plots of the mean squared displacement versus time were used to determine both granular temperature and self-diffusion coefficients [16]. This approach relied on the facts that (a) at times much less than τ_E, the particles move ballistically, resulting in a quadratic variation in the mean squared displacement with time characteristic of the granular temperature; and (b) that this switches to linear behavior given by the two-dimensional equivalent of Eq. (10) at times much longer than τ_E. The current PEPT facility at the University of Birmingham has a temporal resolution, at grains speeds of about 1 m s^{-1}, of about 7 ms, which means that unless the mean free

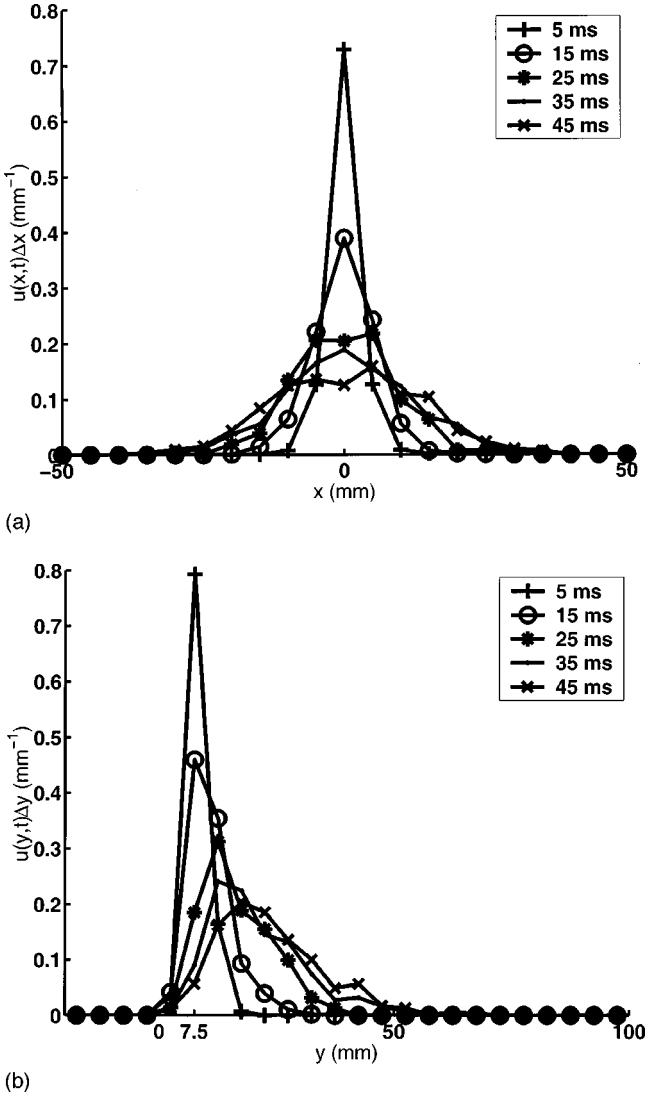

FIG. 5. Displacement probability densities for $N=700$ and $y=7.5$ mm. (a) x component. (b) y component. The spacing $\Delta x=\Delta y=5$ mm.

time between collisions is quite large, i.e., significantly larger than about 7 ms, then it is not possible to calculate granular temperature by analyzing the ballistic region of the mean squared displacement. At low densities, the mean free time between collisions is sufficiently long that analysis of the short time behavior of the grains can provide a value for the granular temperature. For example, Fig. 6 shows the granular temperature profile for a bed of 300 grains vibrated at a shaker amplitude of 2.10 mm. As with the two-dimensional beds considered in Ref. [7], the granular temperature is seen to decay with distance from the base, and, furthermore, the y component of the granular temperature is significantly higher than the x component. However, Fig. 6 implies that the granular temperature in the y direction is depressed at low altitudes, and demonstrates some of the problems inherent in calculating the granular temperature close to the base. This is illustrated by the following simple analysis. When $N=300$, the packing fraction is typically less than 0.02. In three dimensions, and at low packing fractions [i.e., in an ideal Maxwell gas, $g_o(d)\sim 1$], the mean free path λ is related to the packing fraction by [24]

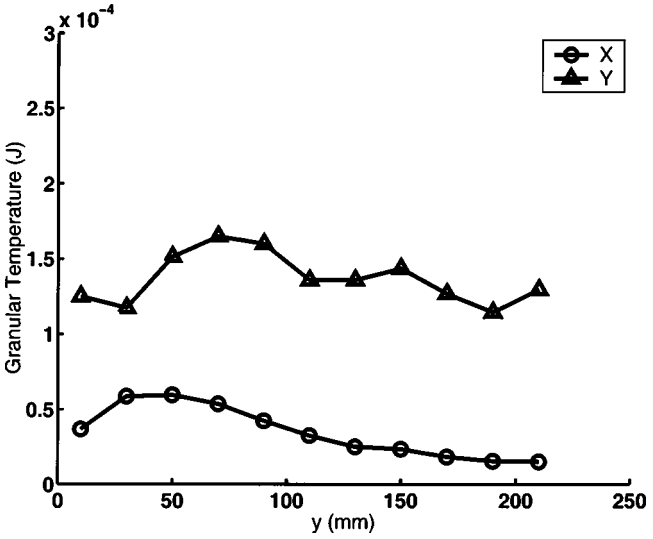

FIG. 6. Granular temperature in the x and y directions, for $N=300$.

$$\lambda=\frac{d}{6\sqrt{2}\,\eta}, \tag{11}$$

suggesting a mean free path of about 30 mm in this low density system. Hence, at positions close to the base (i.e., $y\leqslant 30$ mm) the mean squared displacement will be distorted by the frequent collisions of the grains with the base, and thus leads to lower than expected values for the granular temperature. This highlights the need for careful interpretation of the data in regions in the vicinity of the base.

In this study, the mean squared displacement was measured as a function of height above the base by modifying the method developed to measure the displacement probability density. After the segment number had been determined for each start location, the square of the displacement from that start location was calculated for each subsequent location event. The data were binned into time intervals and a plot of mean squared displacement versus time produced for each time segment. Figure 7 shows the mean squared displacement behavior for a relatively low density system, $N=1050$ [Figs. 7(a) and 7(b)] and a high density system, $N=2450$ [Figs. 7(c) and 7(d)], at two values for the initial height, $y=32.5$ and 52.5 mm, and slice thickness $\Delta y=5$ mm. These plots show the main features observed in all the calculated data sets.

At short times, the average displacement behavior of the grains in each direction is qualitatively indistinguishable: the x and y components of the mean squared displacement tend to follow similar curves. However, at longer times, the differences become apparent. In the low density case, both the x and y components of the mean squared displacement show saturation behavior. In contrast, in the high density case, when saturation becomes apparent, it is restricted to the y component, at least until large heights above the base are investigated.

Examining the low density case first, we observe that the x component of the mean squared displacement saturates at a level equivalent to a root mean squared distance of about 40 mm, regardless of the initial height. The behavior of the y

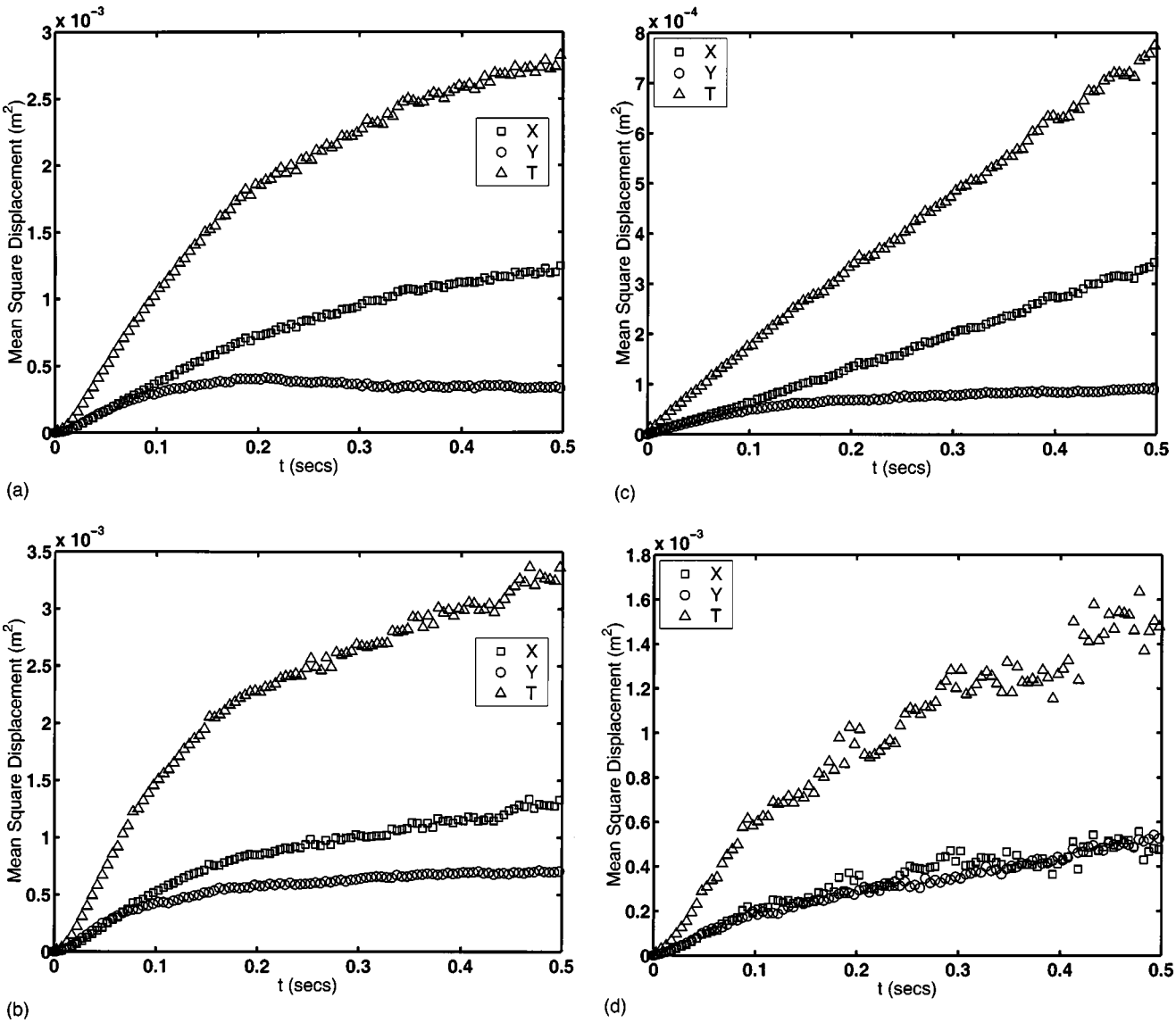

FIG. 7. Mean squared displacement versus time. x and y contributions are shown as squares and circles, respectively, with the total displacement shown as triangles. $N=1050$; start height, $y=$ (a) 32.5 mm and (b) 52.5 mm. $N=2450$; start height, $y=$ (c) 32.5 mm and (d) 52.5 mm.

component of the mean squared displacement is more variable: at low altitudes, saturation tends to occur at mean squared displacements around $10^{-3}\,\mathrm{m}^2$, but this reaches a minimum of about $0.4\times10^{-3}\,\mathrm{m}^2$ at about 32.5 mm from the base. As locations further from the base are examined, the y-direction saturation is seen to rise once more. We suggest that this difference in behavior is due to the fact that the x component of the mean squared displacement is calculated by averaging over all possible start positions, whereas analysis of the y component is restricted to those grains that start in slices 5 mm in thickness, at different altitudes. The motion of the grains in the x direction is not directly influenced by the effect of gravity, and is thus limited only by the physical barriers confining the granular material. As the lateral positioning of the cylinder walls is evidently fixed, it is unsurprising that we observe that the x component of the mean squared displacement should eventually saturate at a fixed distance independent of the starting height. The saturation value for the mean squared x displacement can be calculated straightforwardly by assuming uniform probability densities for both (1) the starting point of a grain, and (2) the long term positions of the grain. The result is $\langle|x(t)-x(0)|^2_{\mathrm{SAT}}\rangle = d_c^2/8$. This suggests a root mean square saturation value of $\sim$50 mm, in reasonable agreement with the value of $\sim$ 40 mm seen in Figs. 7(a) and 7(b).

The corresponding saturation behavior of the y displacement component could, in principle, be calculated from the steady-state packing fraction profiles seen in Fig. 4. Clearly a grain released at $y=32.5$ mm, close to the center of the distribution, will have a smaller maximum mean square displacement than one starting either well below or well above the peak in the packing fraction profile, in qualitative agreement with the observations described earlier.

In the high density system, the saturation occurs in both the x and y directions only at large distances from the base. At positions close to the base, the mean squared displacement is broadly linear with time, indicating that pure diffusive behavior is occurring. Figure 7(c) clearly shows the x

and y components of the mean squared displacement showing contrasting behavior: the x motion remains diffusive, while the y motion shows signs of saturation. In contrast to the behavior in the low density system, in the high density system the x motion remains diffusive up to heights of about 40 mm. The explanation in the low density case was that the side walls limited the mean squared behavior; in the high density system, the packing fraction is higher, the mean path length shorter, and so the mean time taken to collide with the wall is much longer, i.e., the grains in the large-N case were not observed for sufficient time to see saturation. However the depth of the bed is small (compared to the diameter of the experimental cell), and as such there is sufficient time for saturation of the y component of the mean squared displacement to be seen. In the altitude range $y \sim 30-55$ mm, the behavior is somewhat reminiscent of the MD results of Hansen and Helal [25]. In their study of a two-dimensional fluidized granular bed, ''subdiffusive'' behavior was observed in the y direction, with the y component of mean squared displacement rapidly reaching saturation.

D. Convection

Convection currents occur routinely in granular beds undergoing low-amplitude vibration [8], and it is therefore of interest to investigate whether convection is also present in the highly fluidized granular gases considered here. The mean velocity field was calculated by first converting the Cartesian coordinates into a cylindrical coordinate scheme. In the axial direction, the cell was divided into slices, as in Sec. III A. In the radial direction, the cell was split into annuli of equal thickness, and in the ϕ direction (where ϕ is the angle between the projection of the position vector onto the x-z plane and the x axis) the cell was divided into equal sections. As before, each location event was assigned to a volume element. An 11-point finite center-difference approach was used to estimate the mean flow velocity, e.g., in the radial direction

$$v_r(i) = \frac{r(i+5) - r(i-5)}{t(i+5) - t(i-5)}, \tag{12}$$

where $v_r(i)$ is the component of velocity in the r (radial) direction determined for the ith location event. The mean velocity in a segment was then calculated by summing over i for all location events in a segment, and dividing by the number of events attributed to that particular segment. Figure 8 shows the resulting velocity field, in cylindrical coordinates, for a bed containing $N = 2100$ grains, after averaging the velocities in the r and y directions over ϕ, for ease of presentation. Figure 8 shows that while convection is occurring, the mean flow speed is typically less than 0.05 m s^{-1}. This is equivalent to a mean squared displacement of about 6×10^{-6} m^2 after 50 ms, which is evidently small in comparison to the experimentally determined values seen in Figs. 7(a)–7(d), and suggests that the effect of convection on these plots is negligible.

IV. STOCHASTIC BEHAVIOR

It is evident from Figs. 7(a)–7(d) that a granular system is more complicated than the behavior encapsulated in Eq. (10). These differences are driven, at the macroscopic level, by strong gradients in the packing fraction and granular temperature profiles. In order to accommodate this behavior, Eq. (7) needs to be extended and solved with spatially varying coefficients. The governing equation for a system with varying self-diffusion coefficient and under the influence of an external field is given by the so-called Smoluchowski equation, which is a generalization of Eq. (7). In one dimension, the Smoluchowski equation becomes [26]

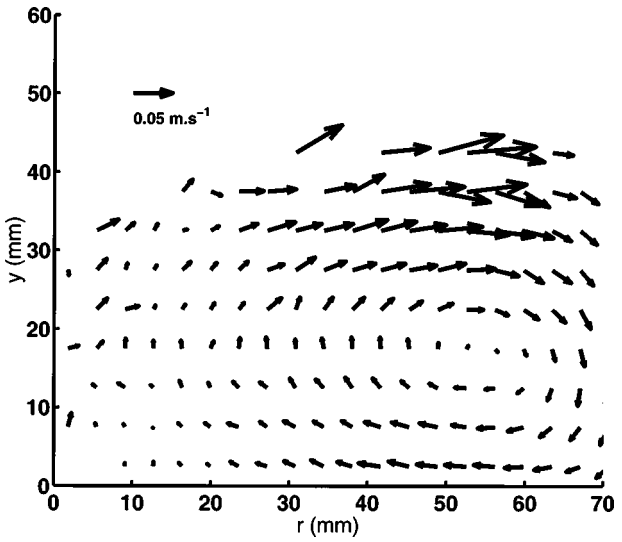

FIG. 8. Mean velocity field for a vibrofluidized granular bed containing $N = 2450$ grains.

$$\frac{\partial u(y,t)}{\partial t} = \frac{\partial}{\partial y}\left\{ D(y)\frac{\partial u(y,t)}{\partial y} + S(y)u(y,t) \right\}, \tag{13}$$

where the coefficient $D(y)$ is the position dependent self-diffusion coefficient, and under conditions for which Chapman-Enskog theory is valid, D can be related to the granular temperature through

$$D(y) = \frac{3}{8n(y)d^2 g_o(d)}\left(\frac{E_O(y)}{\pi m}\right)^{1/2}, \tag{14}$$

where E_O, the granular temperature, is defined by

$$E_O = \tfrac{1}{3}(E_X + E_Y + E_Z) = \tfrac{1}{3}(m\overline{v_X^2} + m\overline{v_Y^2} + m\overline{v_Z^2}), \tag{15}$$

where E_X, E_Y, and E_Z and v_X, v_Y, and v_Z are the granular temperatures and grain velocities in the x, y, and z directions respectively. $S(y)$ is a term that accounts for the acceleration due to gravity between collisions, and can be given by [25]

$$S(y) = \frac{g}{\beta}, \tag{16}$$

where g is the acceleration due to gravity, and β is the friction coefficient. Derivation of the mean squared displacement of a Brownian particle using the Langevin approach [22] results in an expression relating the diffusion coefficient, granular temperature, and friction coefficient:

$$D = \frac{E_0}{\beta m}. \tag{17}$$

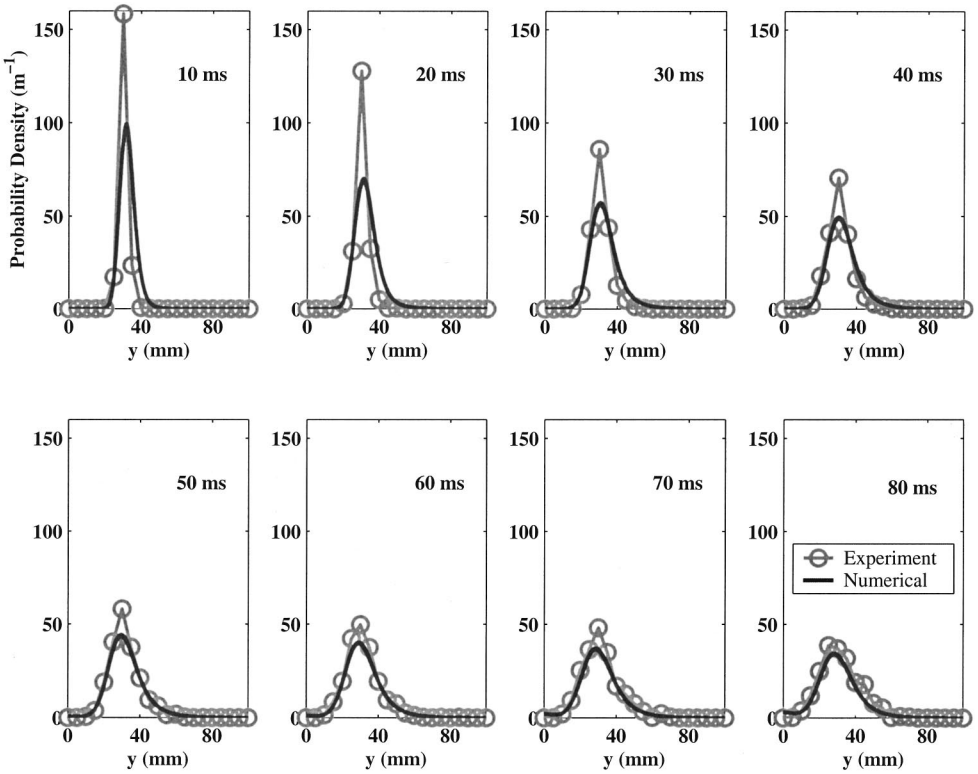

FIG. 9. Comparison of measured and calculated displacement probability density functions ($N=1750$, and the initial height is 30 mm).

Comparison of Eqs. (2), (14), (16), and (17) leads to

$$S(y)=\frac{gd}{16\eta(y)g_o(d)}\left(\frac{E_O(y)}{\pi m}\right)^{-1/2}. \tag{18}$$

As the theoretical forms of the granular temperature and packing fraction are not known, it is not possible to derive an analytical solution to Eq. (13), and hence it must be solved numerically. The approach adopted was to use the measured packing fraction profile $\eta(y)$ and an estimated granular temperature profile $E_O(y)$ to determine $D(y)$ and $S(y)$ via Eqs. (2), (14), and (18). Numerical solution of the differential equation resulted in a prediction for $u(y,t)$ which could then be compared directly with the measured probability density function. The initial estimate for $E_O(y)$ was deduced from measurements of D from the mean squared displacements, e.g., Figs. 7(a)–7(d), and from the packing fraction profile using Eq. (14). $E_O(y)$ was then modified in an iterative way until good agreement was achieved between the predicted and experimental forms for $u(y,t)$.

The method of estimating the solution to Eq. (13) will be discussed in detail in a further publication, but will be described here briefly. The differential equation is approximated using a finite difference equation. It can be shown that a separation of variables solution to the three-dimensional Smoluchowski equation is a set of three independent equations: a one-dimensional Smoluchowski equation in y together with simple diffusion equations (7) in x and z. The PDE describing the motion in the y direction can then be represented using a simple rectilinear mesh representing height and time, with a reflecting boundary at $y=0$. Above the base a second order difference equation is used. At the boundary Neumann derivative boundary conditions assume that the particle flux is zero at the base [26]:

$$D(y)\frac{\partial u(y,t)}{\partial y}+S(y)u(y,t)=0. \tag{19}$$

The Smoluchowski equation describes the spatial development of a system, but it is known that in a vibrofluidized granular system energy is continually being introduced at the base, indicating that an analysis based on the Fokker-Planck equation would be more rigorous [26]. This extension to include velocity space would increase the complexity of the situation several fold. Therefore, as a working hypothesis we make the assumption that the Smoluchowski equation is an adequate model for describing the stochastic development of a granular system, once the steady state granular temperature and packing fraction distribution have been estimated.

The presence of convection currents can in principle lead to problems in the analysis of the system. As discussed in Sec. III D, the presence of convection rolls will cause the flux of grains moving in the vertical direction to vary across the radius of the cell, which could lead to the displacement probability densities becoming artificially widened. However, the y component of the convection current velocity at all but the highest speeds (typically about 0.01 m s^{-1}), leads to a possible extra displacement of the order of 1 mm over 100 ms. This is negligible compared to the distances moved by the grains due to diffusion mechanisms (Fig. 9), and convection was therefore ignored during analysis of the grain motion. Typical results of the analysis are presented in Fig. 9: these show that through the appropriate selection of the granular temperature profile (Fig. 10), close correspondence

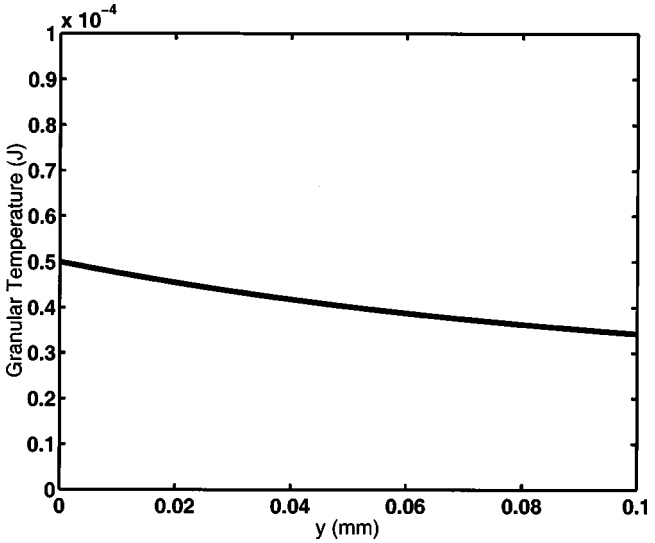

FIG. 10. Granular temperature profile used to generate $D(y)$ and $S(y)$ through Eqs. (14) and (18), respectively.

between the numerical solution of the Smoluchowski equation and the experimental results can be achieved.

V. CONCLUSION

PEPT enables the tracking of a single particle at temporal resolutions (<10 ms) not previously available for analysis of three-dimensional systems. Positron emission tomography and magnetic resonance imaging are both established whole field techniques capable of probing the behavior of quasi-static three-dimensional granular flows, but are not able to resolve motion at the single-particle level in rapidly evolving systems. PEPT was used to analyze the behavior of grains in a three-dimensional vibrofluidized bed. Packing fraction profiles were calculated by making use of the ergodicity of the system. These profiles were qualitatively similar to those seen in two dimensions. Further, stochastic variables such as the mean squared displacement and the displacement probability density functions were determined. Complete velocity fields and indications of convection were observed in continuously vibrated highly fluidised granular beds. At low packing fractions ($\eta<0.4$), the convection currents were sufficiently small to be ignored during analysis of the grain motion. Solution of the Smoluchowski equation using a finite difference approach, and subsequent comparison with experimental results, indicated that such an approach can successfully model a three-dimensional vibrofluidized granular bed.

ACKNOWLEDGMENTS

The work was funded by the Engineering and Physical Sciences Research Council under Contract No. GR/L61781, and by Shell International Oil Products B. V. The authors would like to thank D. Britton for his invaluable technical assistance.

APPENDIX

We assume the vibrofluidized bed to be in a stationary state characterized by a normalized probability distribution function $P_N=P_N(\mathbf{r}_1,\mathbf{p}_1,\ldots,\mathbf{r}_N,\mathbf{p}_N)$ in N-bead phase space. The volume V occupied by the beads is subdivided into n horizontal slices of width $\Delta y=h/n$, where h is the vertical height of the cell. The characteristic function of slice j, $s_j(y)$, may be expressed in terms of the Heaviside step function $\theta(y)$ by

$$s_j(y)=\theta(j\Delta y-y)\,\theta(y-(j-1)\Delta y),\quad 1\leqslant j\leqslant n. \tag{A1}$$

To estimate the mean number N_j of particles in slice j, we introduce the microscopic (dynamical) variable

$$S_j=\sum_{i=1}^{N} s_j(y_i), \tag{A2}$$

where y_i is the vertical coordinate of particle (grain) i. The required mean number N_j is given by the ensemble average of the dynamical variable S_j,

$$N_j=\langle S_j\rangle=\left\langle \sum_{i=1}^{N} s_j(y_i)\right\rangle = N\langle s_j(y_1)\rangle, \tag{A3}$$

since all N grains in the fluidized bed are equivalent. The latter ensemble average may be expressed as

$$N\langle s_j(y_1)\rangle = N\int P_N s_j(y_1)\,d\mathbf{r}_1 d\mathbf{p}_1\cdots d\mathbf{r}_N d\mathbf{p}_N. \tag{A4}$$

The stationary one-particle density $\rho(\mathbf{r}_1)$ is defined as [22]

$$\rho(\mathbf{r}_1)=N\int P_N d\mathbf{p}_1 d\mathbf{r}_2 d\mathbf{p}_2\cdots d\mathbf{r}_N d\mathbf{p}_N, \tag{A5}$$

so that N_j may be re-expressed as

$$\begin{aligned} N_j &= \int \rho(\mathbf{r}_1)s_j(y_1)\,d\mathbf{r}_1 \\ &= A\int \rho(y_1)s_j(y_1)\,dy_1, \end{aligned} \tag{A6}$$

where A is the cross-sectional area of the cell ($V=Ah$), and account was taken of the fact that the grain density profile only depends on the altitude. In summary,

$$\frac{N_j}{N}=\langle s_1(y_1)\rangle=\frac{A}{N}\int_0^h \rho(y)s_j(y)\,dy. \tag{A7}$$

If the stationary state is assumed to be ergodic, N_j may also be expressed as a time average of the dynamical variable [Eq. (A2)] along the phase space trajectory of a single sample,

$$N_j = \lim_{\tau\to\infty}\frac{1}{\tau}\int_0^\tau S_j(t)dt$$

$$= \lim_{\tau\to\infty}\frac{1}{\tau}\int_0^\tau \sum_{i=1}^{N} s_j(y_i(t))dt$$

$$= \lim_{\tau\to\infty}\frac{N}{\tau}\int_0^\tau s_j(y_1(t))dt, \qquad \text{(A8)}$$

where the index 1 denotes the tagged particle, and account was taken once more of the fact that the N grains in the sample are equivalent.

Comparing Eqs. (A7) and (A8), we arrive at the conclusion that the mean fraction of grains found within the horizontal slice $(j-1)\Delta y \leqslant y \leqslant j\Delta y$ is given by

$$F(y) = \frac{N_j}{N} = \frac{A}{N}\int_{(j-1)\Delta y}^{j\Delta y}\rho(y')dy'$$

$$= \lim_{\tau\to\infty}\frac{1}{\tau}\int_0^\tau s_j(y_1(t))dt, \qquad \text{(A9)}$$

allowing the packing fraction to be expressed as a function of the residence time fraction as in Eq. (4).

[1] J. T. Jenkins and S. B. Savage, J. Fluid Mech. **130**, 187 (1983).
[2] S. McNamara and S. Luding, Phys. Rev. E **58**, 813 (1998).
[3] C. S. Campbell, J. Fluid Mech. **348**, 85 (1997).
[4] W. Cooke, S. Warr, J. M. Huntley, and R. C. Ball, Phys. Rev. E **53**, 2812 (1996).
[5] S. B. Savage, J. Fluid Mech. **92**, 53 (1979).
[6] C.-h. Liu and S. R. Nagel, J. Phys.: Condens. Matter **6**, A433 (1994).
[7] S. Warr, G. T. H. Jacques, and J. M. Huntley, Powder Technol. **81**, 41 (1994).
[8] E. E. Ehrichs, H. M. Jaeger, G. S. Karczmar, J. B. Knight, V. Y. Kuperman, and S. R. Nagel, Science **267**, 1632 (1995).
[9] N. Menon and D. J. Durian, Science **275**, 1920 (1997).
[10] D. J. Parker, A. E. Dijkstra, T. W. Martin, and J. P. K. Seville, Chem. Eng. Sci. **52**, 2011 (1997).
[11] J. T. Jenkins and M. Richman, Phys. Fluids **28**, 3485 (1985).
[12] V. Kumaran, J. Fluid Mech. **364**, 163 (1998).
[13] A. Goldshtein and M. Shapiro, J. Fluid Mech. **282**, 75 (1995).
[14] S. Warr, J. M. Huntley, and G. T. H. Jacques, Phys. Rev. E **52B**, 5583 (1995).
[15] S. Warr and J.-P. Hansen, Europhys. Lett. **36**, 589 (1996).
[16] R. D. Wildman and J. M. Huntley, Powder Technol. (to be published).
[17] R. D. Wildman, J. M. Huntley, and J.-P. Hansen, Phys. Rev. E **60**, 7066 (1999).
[18] R. D. Wildman, S. Blackburn, P. McNeil, P. Benton, and D. J. Parker, Powder Technol. **103**, 220 (1999).
[19] D. J. Parker, M. R. Hawkesworth, C. J. Broadbent, P. Fowles, T. D. Fryer, and P. A. McNeil, Nucl. Instrum. Methods Phys. Res. A **348**, 583 (1994).
[20] M. J. Hawkesworth, M. A. Odwyer, J. Walker, P. Fowles, J. Heritage, P. A. E. Stewart, R. C. Witcomb, J. E. Bateman, J. F. Connolly, and R. Stephenson, Nucl. Instrum. Methods Phys. Res. A **253**, 145 (1986).
[21] K. Helal, T. Biben, and J.-P. Hansen, Physica A **240**, 361 (1997).
[22] J. P. Hansen and I. R. McDonald, *Theory of Simple Liquids*, 2nd ed. (Academic, London, 1986).
[23] N. F. Carnahan and K. E. Starling, J. Chem. Phys. **11**, 635 (1969).
[24] S. G. Starling and A. J. Woodall, *Physics*, 2nd ed. (Longmans, London, 1957).
[25] J.-P. Hansen and K. Helal, in *Turbulence et Déterminsme*, edited by M. Lesieur (Presses Universitaires de Grenoble, Grenoble, 1998).
[26] S. Chandrasekhar, in *Noise and Stochastic Processes*, edited by N. Wax (Dover, New York, 1954).